Dipole-dipole interaction between a quantum dot and a graphene nanodisk

Joel D. Cox,[1] Mahi R. Singh,[1] Godfrey Gumbs,[2] Miguel A. Anton,[3] and Fernando Carreno[3]
[1]*Department of Physics and Astronomy, The University of Western Ontario, London, Canada N6A 3K7*
[2]*Department of Physics and Astronomy, Hunter College at the City University of New York, New York 10065, USA*
[3]*Escuela Universitaria de Optica, Universidad Complutense de Madrid, Madrid 28037, Spain*
(Received 4 June 2012; revised manuscript received 3 August 2012; published 28 September 2012; corrected 28 January 2013)

We study theoretically the dipole-dipole interaction and energy transfer in a hybrid system consisting of a quantum dot and graphene nanodisk embedded in a nonlinear photonic crystal. In our model, a probe laser field is applied to measure the energy transfer between the quantum dot and graphene nanodisk, while a control field manipulates the energy transfer process. These fields create excitons in the quantum dot and surface plasmon polaritons in the graphene nanodisk which interact via the dipole-dipole interaction. Here, the nonlinear photonic crystal acts as a tunable photonic reservoir for the quantum dot, and is used to control the energy transfer. We have found that the spectrum of power absorption in the quantum dot has two peaks due to the creation of two dressed excitons in the presence of the dipole-dipole interaction. The energy transfer rate spectrum of the graphene nanodisk also has two peaks due to the absorption of these two dressed excitons. Additionally, energy transfer between the quantum dot and the graphene nanodisk can be switched on and off by applying a pump laser to the photonic crystal or by adjusting the strength of the dipole-dipole interaction. We show that the intensity and frequencies of the peaks in the energy transfer rate spectra can be modified by changing the number of graphene monolayers in the nanodisk or the separation between the quantum dot and graphene. Our results agree with existing experiments on a qualitative basis. The principle of our system can be employed to fabricate nanobiosensors, optical nanoswitches, and energy transfer devices.

DOI: 10.1103/PhysRevB.86.125452 PACS number(s): 78.67.Hc, 73.20.Mf, 78.67.Wj

I. INTRODUCTION

There has been growing interest in developing nanoscale optoelectronic devices by combining nanomaterials with complementary optical properties into composite (hybrid) structures. The number of possible composite systems that can be built from already existing nanostructures is simply enormous. A significant amount of research on nanocomposites has been devoted to the study of exciton-plasmon interactions in metal-semiconductor nanostructures, which offer a wide range of opportunities to control light-matter interactions and electromagnetic energy flows on nanometer length scales.[1–6] Strong exciton-surface plasmon coupling in semiconductor quantum-dot (QD) metal nanoparticle systems could lead to efficient transmission of quantum information between qubits for applications in quantum computing and communication.[2] These nanostructures also have applications in biophotonics and sensing, where nonradiative energy transfer between a QD and metal nanoparticle can be used to detect biological molecules.[3]

In this paper, we study theoretically the dipole-dipole interaction (DDI) and energy transfer between a quantum emitter and a graphene nanodisk. The quantum emitter can be a quantum dot, nanocrystal, or a chemical or biological molecule. Here, the quantum emitter-graphene system is embedded in a photonic crystal, which acts as a tunable photonic reservoir for the emitter. Photonic crystals are engineered, periodically ordered microstructures that facilitate the trapping and control of light on the microscopic level. Applications for photonic crystals include all-optical microchips for optical information processing, optical communication networks, sensors, and solar energy harvesting.[7–12] In our investigation, we consider a nonlinear photonic crystal, which has a refractive index distribution that can be tuned optically. The nonlinear photonic crystal surrounds the hybrid system and is used to manipulate the interaction between the quantum emitter and graphene nanodisk.

Surface plasmon polaritons are created in the graphene nanodisk due to the collective oscillations of conduction-band electrons. They arise due to the dielectric contrast between graphene and the surrounding dielectric medium. Plasmonics is widely studied due to applications in ultrasensitive optical biosensing,[13] photonic metamaterials,[14] light harvesting,[15] optical nanoantennas,[16] and quantum information processing.[17] Generally, noble metals are considered as the best available materials for the study of surface plasmon polaritons.[18] However, noble metals are hardly tunable and exhibit large Ohmic losses, which limit their applicability to optical processing devices. Graphene plasmons provide an attractive alternative to noble-metal plasmons, as they exhibit much tighter confinement and relatively long propagation distances. Furthermore, surface plasmons in graphene have the advantage of being highly tunable via electrostatic gating. Compared to noble metals, graphene also has superior electronic and mechanical properties, which originate in part from its charge carriers of zero effective mass.[19] For example, charge carriers in graphene can travel for micrometers without scattering at room temperature. Graphene has also been recognized as a useful optical material for novel photonic and optoelectronic applications.[20–25] For these reasons, the study of plasmonics in graphene has received significant attention both experimentally and theoretically.[21,22,26–29]

Recently, experimental research on graphene has been extended to the fabrication and study of QD-graphene nanostructures.[30–34] For example, a CdS QD-graphene hybrid system has been synthesized by Cao *et al.*,[30] in which a picosecond ultrafast electron transfer process from the

excited QD to the graphene matrix was observed using time-resolved fluorescence spectroscopy. Chen *et al.*[31] have fabricated CdSe/ZnS QDs in contact with single- and few-layer graphene sheets. By measuring the strong quenching of the QD fluorescence, they determined the rate of energy transfer from the QD to graphene. A similar study by Dong *et al.*[32] was performed on a CdTe QD and graphene oxide system, but in their case the QDs were modified with molecular beacons in order to demonstrate that the hybrid system can be used for sensing biological molecules. Wang *et al.*[33] have synthesized graphene-CdS and graphene-ZnS QD hybrid systems directly from graphene oxide, with CdS and ZnS QDs very well dispersed on the graphene nanosheets. They also measured the QD photoluminescence and observed the energy transfer between the QDs and graphene. Metal nanoparticle-graphene hybrid systems have also been fabricated by several groups.[21,35–37]

Here, we study a QD-graphene hybrid system, where energy transfer occurs due to the interaction between optical excitations in the QD and graphene nanodisk. The optical excitations in the QD are excitons, which are electron-hole pairs, while those in the graphene nanodisk are surface plasmon polaritons, which are created due to the collective oscillations of conduction-band electrons. The QD is taken as a three-level lambda-type system in which two distinct excitonic transitions occur. Other three-level systems in the ladder-[3] and V-type[38] configurations interacting with a metallic nanoparticle in the presence of two external fields have been studied. In our model, we include a probe laser field which is coupled with one excitonic transition and measures the energy transfer spectra of the QD and graphene. We also consider that a control laser field is applied to monitor and control the energy transfer. Aside from creating excitons in the QD, these fields also generate surface plasmon polaritons in graphene. The dipoles created by excitons in the QD and plasmons in the graphene nanodisk then interact via the DDI. This interaction is strong when the QD and graphene are in close proximity and their optical excitation frequencies are resonant.

We have found that the power absorption spectrum of the QD has two peaks when the QD and graphene nanodisk are in close proximity, indicating the creation of two dressed excitons due to the DDI. These dressed excitons are transported to graphene, and produce two peaks in the spectrum of the energy transfer rate to graphene. We show that the energy transfer between the QD and graphene can be switched on and off by changing the strength of the DDI coupling or by applying an intense laser field to the nonlinear photonic crystal. The intensities of peaks in the energy transfer rate spectra can be controlled by changing the number of graphene monolayers or by changing the distance between the QD and graphene. We have also predicted that the intensity of these peaks can be modified in the presence of biological materials. Our findings agree with the experimental results of Refs. 30–34 on a qualitative basis. The present system can be used to fabricate nanobiosensors, all-optical nanoswitches, and energy transfer devices.

II. THEORETICAL FORMALISM

We investigate theoretically the dipole-dipole interaction and energy transfer between a quantum dot and graphene

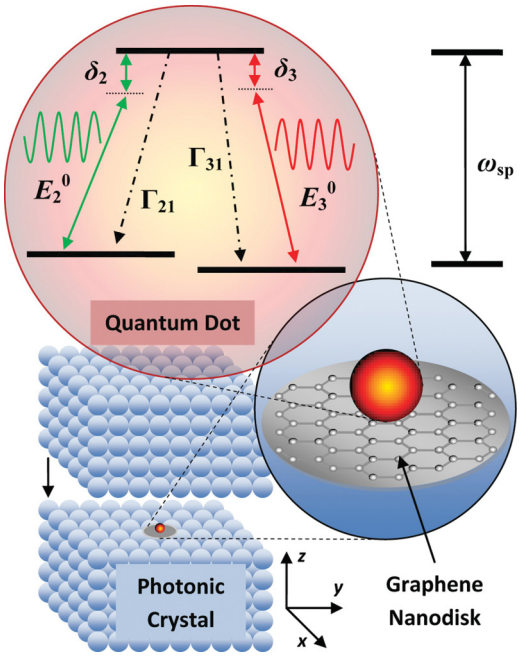

FIG. 1. (Color online) A schematic diagram of the QD-graphene nanocomposite embedded in a photonic crystal. The QD has three discrete states, where $|2\rangle$ and $|3\rangle$ denote the lower-energy states, which are near degenerate and are both coupled to the common optically excited state $|1\rangle$.

nanodisk when the system is embedded in a nonlinear photonic crystal. A schematic diagram for the present system is shown in Fig. 1. A graphene nanodisk (or nanoflake) lies in the x-y plane, on top of which a QD is deposited. The center-to-center distance between the QD and graphene nanodisk is taken as R. The combined QD-graphene nanodisk system can also be referred to as a QD-graphene nanocomposite or hybrid system. The QD considered here has three discrete states, where $|2\rangle$ and $|3\rangle$ are the lower-energy states which are near degenerate and both coupled to the common optically excited state $|1\rangle$. The QD acts as a three-level quantum emitter, where excitons are created by the transitions $|2\rangle \leftrightarrow |1\rangle$ and $|3\rangle \leftrightarrow |1\rangle$ with resonance frequencies (dipole moments) ω_{12} (μ_{12}) and ω_{13} (μ_{13}), respectively. This so-called Lambda-type energy-level configuration has been widely studied in atoms, where quantum optical effects such as electromagnetically induced transparency and coherent population trapping have been demonstrated.[39,40] More recently, this energy-level configuration has been achieved in semiconductor QDs.[41–43] The distance between the quantum dot and graphene can be changed by using the following methods: (a) by using a passive dielectric spacer between the quantum dot and graphene, (b) using quantum dots with different diameters, (c) by applying an external stress or strain fields to the system, and (d) by changing the concentration of quantum dots or graphene nanodisks.

In our model, we consider that a probe field $E_2 = E_2^0 \cos(\omega_2 t)$ is applied between states $|1\rangle$ and $|2\rangle$. To control the coupling between the QD and graphene, a control field $E_3 = E_3^0 \cos(\omega_3 t)$ is applied between states $|1\rangle$ and $|3\rangle$. These laser fields excite both the QD and graphene nanodisk. In the QD, the probe and control fields create excitons which

produce dipole electric fields that interact with the graphene nanodisk. Similarly, in the graphene nanodisk, surface plasmon polaritons are generated by the probe and control fields, which produce dipole electric fields that interact with the QD. Surface plasmon polaritons in graphene are evanescent electromagnetic waves (TM modes) induced by the coupling of TM modes with the two-dimensional collective excitations (plasmons) in graphene. The amplitude of the surface plasmon polaritons decays exponentially on either side of the interface between graphene and the surrounding dielectric photonic crystal.

The dipole electric fields produced by the QD and graphene are written as

$$E_{\mathrm{DDI}}^{\mathrm{QD}} = \frac{g_l P_{\mathrm{QD}}}{4\pi\epsilon_b R^3}, \qquad E_{\mathrm{DDI}}^{G} = \frac{g_l P_G}{4\pi\epsilon_b R^3}, \tag{1}$$

respectively. Here, $\epsilon_{bd} = (2\epsilon_b + \epsilon_d)/3\epsilon_b$, where ϵ_d is the dielectric constant of the QD and ϵ_b is the dielectric constant of the medium surrounding the QD-graphene system. The parameter g_l ($l = x, y, z$) is the polarization parameter, with $g_x = g_y = -1$ and $g_z = 2$ for electric fields polarized in the x-y plane or in the z direction, respectively.[44] In Eq. (1), P_{QD} and P_G are the polarization of the quantum dot and graphene nanodisk, respectively. The polarization of the QD is obtained as

$$P_{\mathrm{QD}} = \sum_{i=2,3} \mu_{1i}(\rho_{1i} + \rho_{i1}), \tag{2}$$

where μ_{ij} and ρ_{ij} are the dipole moment and density matrix element, respectively, for the transition $|i\rangle \leftrightarrow |j\rangle$.

The total electric field felt by the graphene nanodisk is written as

$$E_G = E_2 + E_3 + E_{\mathrm{DDI}}^{\mathrm{QD}}, \tag{3}$$

where the first, second, and third terms are the contributions from the probe, control, and the QD dipole field, respectively. Using the quasistatic dipole approximation,[44] the polarization in the graphene nanodisk is

$$P_G = \epsilon_b \alpha_l \left(E_2 + E_3 + E_{\mathrm{DDI}}^{\mathrm{QD}}\right), \tag{4}$$

$$\alpha_l = \frac{4\pi L_x L_y L_z [\epsilon_m(\omega) - \epsilon_b]}{3\epsilon_b + 3\varsigma_l[\epsilon_m(\omega) - \epsilon_b]}, \tag{5}$$

where α_l is the polarizability of the graphene nanodisk and $\epsilon_g(\omega)$ denotes the dielectric function of graphene. Here, ς_l is called the depolarization factor and is obtained as

$$\varsigma_l = \frac{L_x L_y L_z}{2} \int_0^\infty \frac{dq}{\left(L_l^2 + q\right) f(q)}, \tag{6}$$

where

$$f(q) = \sqrt{\left(L_x^2 + q\right)\left(L_y^2 + q\right)\left(L_z^2 + q\right)}. \tag{7}$$

The depolarization parameters satisfy the relation $\varsigma_x + \varsigma_y + \varsigma_z = 1$, and determine the optical response of the graphene nanodisk based on its shape.[44] For an oblate spheroid where $L_x = L_y$ and $L_x > L_z$, the depolarization factors reduce to

$$\varsigma_z = \frac{1 - e_g^2}{e_g^2}\left[\frac{1}{2e_g}\ln\left(\frac{1 + e_g}{1 - e_g}\right) - 1\right], \qquad \varsigma_x = \varsigma_y = \frac{1}{2}(1 - \varsigma_z), \tag{8}$$

where the eccentricity of the nanodisk is defined as $e_g = \sqrt{1 - (L_x/L_z)^2}$. Note that this equation is valid for both cases where $L_x > L_z$ and $L_x < L_z$.[44]

The above expression for the polarizability given in Eq. (5) has been widely used in the literature to study the optical properties of metallic nanodisks, and has been found to give good agreement with experimental results.[45,46] In the quasistatic approximation, the dimensions of the graphene nanodisk are much smaller than the wavelength of incident light and we therefore assume a spatially uniform but time-varying electric field across the graphene nanodisk. Here, the wavelengths of light considered are on the order of several hundred nanometers, and thus the size of the graphene nanodisk must be less than 100 nm. It is important to note that our model is only valid for nanosize graphene samples and not for bulk materials. For a very flat and thin disk, we take $L_x \gg L_z$, which gives[47,48]

$$\varsigma_x = \varsigma_y \cong \frac{\pi}{4}\frac{L_z}{L_x}, \qquad \varsigma_z \cong 1 - \frac{\pi}{2}\frac{L_z}{L_x}. \tag{9}$$

The above method has been used for a graphene flake in Ref. 49.

The total electric field felt by the QD is written as

$$E_{\mathrm{QD}} = \frac{E_2}{\epsilon_{bd}} + \frac{E_3}{\epsilon_{bd}} + \frac{g_l \alpha_l \left(E_2 + E_3 + E_{\mathrm{DDI}}^{\mathrm{QD}}\right)}{4\pi\epsilon_{bd} R^3}, \tag{10}$$

where the first, second, and third terms are the contributions from the probe, control, and the graphene dipole field, respectively. Putting the expression of $E_{\mathrm{DDI}}^{\mathrm{QD}}$ from Eq. (1) into the above expression, we get

$$E_{\mathrm{QD}} = \sum_{i=2,3}\left(E_F^i + E_{\mathrm{DDI}}^i\right), \qquad E_F^i = \frac{\hbar}{\mu_{1i}}\Omega_i e^{-i\omega_i t} + \mathrm{c.c.}, \qquad E_{\mathrm{DDI}}^i = \frac{\hbar}{\mu_{1i}}(\Pi_i + \Lambda_i \rho_{1i}) e^{-i\omega_i t} + \mathrm{c.c.}, \tag{11}$$

where

$$\Omega_i = \frac{\mu_{1i} E_i^0}{2\hbar\epsilon_{bd}}, \quad \Pi_i = \frac{g_l \alpha_l(\omega_i)\Omega_i}{4\pi R^3}, \quad \Lambda_i = \frac{g_l^2 \alpha_l(\omega_i)\mu_{1i}^2}{(4\pi)^2 \epsilon_b \hbar \epsilon_{bd}^2 R^6}. \tag{12}$$

The dipoles of the QD interact with the dipole electric field produced by the graphene nanodisk, and vice versa. This interaction is called the dipole-dipole interaction. The terms in the interaction Hamiltonian of the QD due to the external probe and control fields and the DDI are expressed in the rotating

wave approximation as

$$H_{\text{QD-}F} = -\sum_{i=2,3} \mu_{1i} E_F^i \sigma_{1i}^+ + \text{H.c.}$$
$$H_{\text{QD-DDI}} = -\sum_{i=2,3} \mu_{1i} E_{\text{DDI}}^i \sigma_{1i}^+ + \text{H.c.} \quad (13)$$

Using the expressions for E_F^i and E_{DDI}^i in Eqs. (11) in the above expression and putting the Hamiltonian in interaction representation, we get

$$H_{\text{QD-}F} = -\sum_{i=2,3} \hbar\Omega_i \sigma_{1i}^+ e^{-i(\omega_i-\omega_{1i})t} + \text{H.c.},$$
$$H_{\text{QD-DDI}} = -\sum_{i=2,3} \hbar(\Pi_i + \Lambda_i \rho_{1i}) \sigma_{1i}^+ e^{-i(\omega_i-\omega_{1i})t} + \text{H.c.}, \quad (14)$$

where $\sigma_{ij}^+ = |i\rangle\langle j|$ ($\sigma_{ij} = |j\rangle\langle i|$) is the exciton creation (annihilation) operator. The interaction Hamiltonian term $H_{\text{QD-}F}$ given in Eq. (14) represents the direct contribution from the external probe ($i = 2$) and control ($i = 3$) fields incident on the QD, and is given in terms of the Rabi frequencies Ω_i, which measure the intensities of these fields. The second contribution $H_{\text{QD-DDI}}$ represents the fields incident on the QD due to the DDI between the QD and graphene nanodisk, and contains two terms Π_i and $\Lambda_i \rho_{1i}$. The first DDI term is due to the interaction of the QD with the dipole electric fields from the graphene nanodisk induced by the probe and control fields. Therefore, we refer to this as the *direct DDI* term. The second DDI contribution is due to the interaction of the QD with a dipole field from graphene that arises when the external fields polarize the QD, which in turn polarize graphene. In other words, these contributions are the self-interaction of the QD, as they depend on the polarization of the QD. For this reason, this term is called the *self-induced DDI* parameter. The surface plasmon polariton resonance frequency ω_{sp}^l in the graphene nanodisk is obtained by setting the real part of the denominator in $\alpha_l(\omega)$ equal to zero and solving for ω. When the optical excitation frequencies of the QD lie near the surface plasmon polariton resonance frequencies of the graphene nanodisk (i.e., $\omega_{1i} \approx \omega_{sp}$), the DDI becomes very strong due to the enhanced local fields in the vicinity of the graphene nanodisk. This interaction leads to excitation and energy transfer between the QD and graphene.

The combined QD-graphene system is embedded in a photonic crystal consisting of dielectric spheres arranged periodically in three dimensions, which acts as a reservoir for the QD. Therefore, we consider that the excited state $|1\rangle$ spontaneously decays to the lower-energy states $|2\rangle$ and $|3\rangle$ due to excitons coupling with Bloch photons in the photonic crystal (see Fig. 1). In this case, the interaction Hamiltonian is given as

$$H_{\text{QD-PC}} = -\sum_{i=2,3}\sum_k g_{1i}^{\text{PC}} a_k \sigma_{1i}^+ e^{i(\omega_{1i}-\omega_k)t} + \text{H.c.},$$
$$g_{1i}^{\text{PC}} = \sqrt{\frac{\hbar\omega_k}{2\epsilon_b V_{PC}}}(\mathbf{e}_k \cdot \mu_{1i}), \quad (15)$$

where $\mathbf{e}_k$ is the polarization unit vector of the Bloch photons in the PC, and V_{PC} is the volume of the photonic crystal. The operator a_k^+ (a_k) is the photon creation (annihilation) operator, while ω_k and k are the Bloch photon frequency and wave vector, respectively.

Finally, the total interaction Hamiltonian of the system is written as

$$H = H_{\text{QD-}F} + H_{\text{QD-DDI}} + H_{\text{QD-PC}}$$
$$= -\sum_{i=2,3} \hbar(R_i e^{i\theta_i} + \Lambda_i \rho_{1i}) \sigma_{1i}^+ e^{-i(\omega_i-\omega_{1i})t}$$
$$- \sum_{i=2,3}\sum_k g_{1i}^{\text{PC}} a_k \sigma_{1i}^+ e^{i(\omega_{1i}-\omega_k)t} + \text{H.c.}, \quad (16)$$

where

$$R_i = \sqrt{[\Omega_i + \text{Re}(\Pi_i)]^2 + [\text{Im}(\Pi_i)]^2},$$
$$\theta_i = \arctan\left[\frac{\text{Im}(\Pi_i)}{\Omega_i + \text{Re}(\Pi_i)}\right].$$

Note that the first term in the above expression for H is the combination of $H_{\text{QD-}F}$ with the direct DDI term.

We use the density matrix method to evaluate the energy transfer between the QD and the graphene. Using Eq. (16) for the interaction Hamiltonian and the master equation for the density matrix,[39] we obtained the following equations of motion for the QD density matrix elements as

$$\frac{d\rho_{22}}{dt} = 2\Gamma_{21}\rho_{11} - iR_2 e^{i\theta_2}\rho_{21} - i\Lambda_2\rho_{12}\rho_{21} + iR_2 e^{-i\theta_2}\rho_{12} + i\Lambda_2^*\rho_{21}\rho_{12}, \quad (17)$$

$$\frac{d\rho_{33}}{dt} = 2\Gamma_{31}\rho_{11} - iR_3 e^{i\theta_3}\rho_{31} - i\Lambda_3\rho_{13}\rho_{31} + iR_3 e^{-i\theta_3}\rho_{13} + i\Lambda_3^*\rho_{31}\rho_{13}, \quad (18)$$

$$\frac{d\rho_{12}}{dt} = -d_{12}\rho_{12} + iR_3 e^{i\theta_3}\rho_{32} + i\Lambda_3\rho_{13}\rho_{32} - iR_2 e^{-i\theta_2}(\rho_{11} - \rho_{22}), \quad (19)$$

$$\frac{d\rho_{13}}{dt} = -d_{13}\rho_{13} + iR_2 e^{i\theta_2}\rho_{23} + i\Lambda_2\rho_{12}\rho_{23} - iR_3 e^{i\theta_3}(\rho_{11} - \rho_{33}), \quad (20)$$

$$\frac{d\rho_{23}}{dt} = -i(\delta_2 - \delta_3)\rho_{23} + iR_2 e^{-i\theta_2}\rho_{13} + i\Lambda_2^*\rho_{21}\rho_{31} - iR_3 e^{i\theta_3}\rho_{21} - i\Lambda_3\rho_{13}\rho_{21}, \quad (21)$$

where

$$d_{1i} = \Gamma_{21} + \Gamma_{31} - \Gamma_{id} - i\Delta_{id} - i\delta_i,$$
$$\delta_i = \omega_i - \omega_{1i}.$$

Here, δ_i are the detuning of the probe ($i = 2$) and control ($i = 3$) fields. Note that the diagonal elements of the density matrix satisfy the relation $\rho_{11} + \rho_{22} + \rho_{33} = 1$. The quantities Γ_{id} and Δ_{id} are the *nonradiative decay rate* and *energy shift*, respectively, due to self-induced DDI parameters Λ_i. They are found as

$$\Gamma_{id} = \text{Im}(\Lambda_i)(\rho_{ii} - \rho_{11}),$$
$$\Delta_{id} = \text{Re}(\Lambda_i)(\rho_{ii} - \rho_{11}).$$

The parameters Γ_{i1} represent the spontaneous decay rates of excited state $|1\rangle$ to state $|i\rangle$ due to the Bloch photons in the

photonic crystal, and are given as

$$\Gamma_{i1} = \Gamma_{i1}^0 \frac{\pi^2 c^3}{V_{\rm PC}\omega_{1i}^2} D(\omega_{1i}), \tag{22}$$

where

$$D(\omega) = \sum_{\pm} \frac{\xi_{\pm}^0(\omega) V_{\rm PC} \arccos^2[F(\omega)]}{\sqrt{1-F^2(\omega)}},$$

$$\xi_{\pm}^0(\omega) = \frac{(n_a \pm n_b)^2 (n_a a \pm n_b b)}{2\pi^2 L^3 c n_a n_b} \sin\left[\frac{2\omega}{c}(n_a a \pm n_b b)\right],$$

and

$$F(\omega) = \sum_{\pm} \pm \frac{(n_a \pm n_b)^2}{4 n_a n_b} \cos\left[\frac{2\omega}{c}(n_a a \pm n_b b)\right].$$

In the above expression, Γ_{i1}^0 is the exciton decay rate due to the background radiation field in free space. Here, $L = 2a + 2b$ is the photonic crystal lattice constant, $2b$ is the spacing between dielectric spheres, and a is the radius of the spheres. Parameters n_a and n_b denote the refractive index of the dielectric spheres and background material in the photonic crystal, respectively. The expression for the photonic density of states $D(\omega)$ has been derived in Ref. 50. Here, we have used the Markovian approximation in order to derive the decay rates for the QD in the presence of the photonic crystal. This approximation ignores memory effects in the electromagnetic reservoir due to the presence of the QD, and is valid when the photonic density of states can be considered smooth and slowly varying compared to the energy difference between the edge of the photonic band gap and the resonance frequency of the QD.[51] Note that in our calculations, we remain within the regime where the Markovian approximation is valid. Therefore, the effect of the photonic crystal serves only to alter the decay rates of the excitonic transitions compared to those in free space. We numerically solve Eqs. (17)–(21) by first substituting $\rho_{12} = \widetilde{\rho}_{12} e^{i\theta_2}$, $\rho_{13} = \widetilde{\rho}_{13} e^{i\theta_3}$, and $\rho_{23} = \widetilde{\rho}_{23} e^{-i(\theta_2-\theta_3)}$.

Following the method of Ref. 44 and using Eq. (16), the energy absorption rate of the QD ($W_{\rm QD}$) and the energy transfer rate from the QD to graphene (W_G) are found as

$$W_{\rm QD} = \sum_{i=2,3} \hbar\omega_{1i}\rho_{11}\Gamma_{i1}, \tag{23}$$

$$W_G = \sum_{i=2,3} \frac{g_{x,z}^2 \mu_{1i}^2 \omega_i {\rm Im}(\alpha_x) |\widetilde{\rho}_{1i}|^2}{8\pi^2 \epsilon_b \epsilon_{bd}^2 |\epsilon_{bg}|^2 R^6}, \tag{24}$$

where $\epsilon_{bg} = (2\epsilon_b + \epsilon_g)/3\epsilon_b$. The expression for $W_{\rm QD}$ is obtained by assuming that the power radiated from the QD is equal to its energy absorption rate. Similar expressions have been widely used in the literature on hybrid systems.[2,3] Note that the energy transfer to graphene depends on the coherences $\widetilde{\rho}_{1i}$ of the QD density matrix, which change depending on the center-to-center distance between the QD and graphene R. Therefore, Eq. (24) does not simply depend on R^6, but rather is a much more complicated function of R.

III. RESULTS AND DISCUSSION

In the literature, the size of the graphene nanodisk should not be less than 10 nm in diameter for the edge effects to be neglected (Ref. 52). In this paper, we consider a graphene nanodisk with diameter 14 nm. The thickness of the nanodisk is $L_z = 0.35$ nm (i.e., a single graphene layer) and its size ratio $L_x/L_z = 20$. The plasmon frequency and background dielectric constant of graphene are taken from experiments as 6.02 eV and 1.964, respectively.[21] The decay rate in graphene is taken as $\gamma_G = 5$ THz, which is consistent with the relaxation rates reported in Refs. 22 and 26. With these parameters, the surface plasmon polariton resonance frequencies in the graphene nanodisk are calculated as $\hbar\omega_{sp}^x = 0.8026$ eV and $\hbar\omega_{sp}^z = 4.1250$ eV. The QD dielectric constant and dipole moments are taken as $\epsilon_d = 12$ and $\mu_{12} = \mu_{13} = 0.1\ e \times$ nm, respectively, while the free-space decay rates for the QD are taken as $\Gamma_{21}^0 = \Gamma_{31}^0 = 0.2\ \mu$eV. These parameters are comparable to those commonly found in the literature for QDs.[2–4] Here, the transition energies in the QD are taken to lie near the plasmon resonance $\hbar\omega_{sp}^x$ as $\hbar\omega_{12} = 0.8046$ eV and $\hbar\omega_{13} = 0.8036$ eV. The combined QD-graphene nanodisk hybrid is contained within a photonic crystal made of polystyrene spheres arranged periodically in air. Similar photonic crystals have been fabricated by Liu *et al.*[9] in which ultrafast all-optical switching was experimentally demonstrated. Photonic crystal parameters are taken as $a = 170$ nm, $L = 480$ nm, $n_a = 1.59$, and $n_b = 1$. With these parameters, we find that a photonic band gap appears between frequencies 0.8225 and 0.9843 eV. Note that the lower edge of the band gap lies near ω_{sp}^x and the QD transition frequencies ω_{12} and ω_{13}. The vacuum decay rates for the QD are taken as $\Gamma_2^0 = \Gamma_3^0 = 0.2\ \mu$eV, and in the presence of the photonic crystal it is found that $\Gamma_{21} = 1.1370\ \mu$eV and $\Gamma_{31} = 1.1127\ \mu$eV. Here, the background dielectric constant was taken as $\epsilon_B = 2.081$. Throughout the following calculations, we consider that the intensity of the probe and control fields are 1.0 and 3.0 W/cm^2, respectively.

We first consider the case where the excitonic transition $|3\rangle \leftrightarrow |1\rangle$ is coupled with the surface plasmon resonance of the graphene nanodisk. In this configuration, the transition frequency ω_{13} is near ω_{sp}^x, while both the control field E_3 and the transition dipole moment μ_{13} are polarized in the x-y plane. Conversely, the transition $|2\rangle \leftrightarrow |1\rangle$ is not coupled with the graphene nanodisk. This situation occurs when the probe field E_2 and transition dipole moment μ_{12} are polarized in the z direction and ω_{12} is far away from ω_{sp}^z (see Fig. 2 inset). The energy absorption rate in the QD is evaluated from Eq. (23) and the results are presented in Fig. 2(a) when the QD-graphene separation R is varied and the control field is resonant with the $|3\rangle \leftrightarrow |1\rangle$ transition such that $\delta_3 = 0$. It is found that the power absorption spectrum has a single peak with an extremely narrow transparent window at $\delta_2 = 0$ when the QD and graphene are further away from each other (i.e., $R = 20$ nm). These narrow minima are due to electromagnetically induced transparency in the system. When the QD is close to graphene (i.e., $R = 8$ nm), the power absorption peak splits into two peaks and a clear minimum appear at $\delta_2 = 0$. The observed splitting is due to the DDI and surface plasmon polariton coupling.

The splitting of the power absorption spectrum can be explained using the theory of dressed states. When the QD is close to the graphene nanodisk, there is strong coupling due to the DDI for the transition $|3\rangle \leftrightarrow |1\rangle$. This causes the excited state $|1\rangle$ to split into two dressed states, namely, $|1_+\rangle$ and $|1_-\rangle$. Therefore, there are now two transitions $|2\rangle \leftrightarrow |1_+\rangle$ and $|2\rangle \leftrightarrow |1_-\rangle$ which give two peaks and a minimum in the

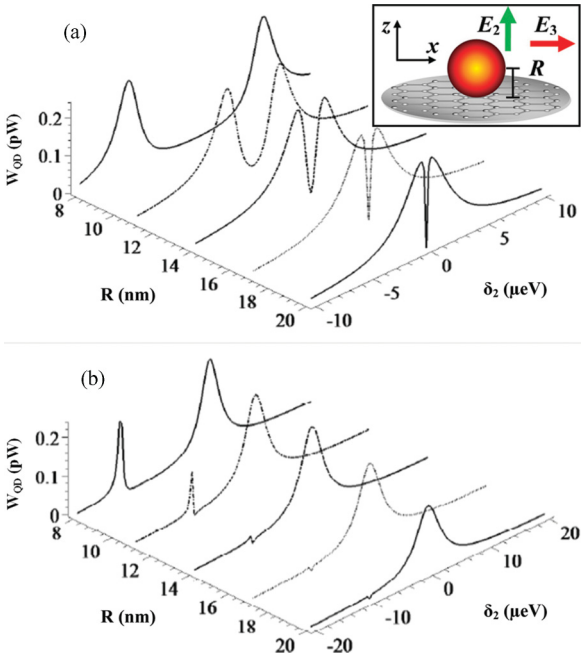

FIG. 2. (Color online) Energy absorption rate of the QD as a function of probe field detuning δ_2 when the QD-graphene nanodisk separation R is varied. (a) $\delta_3 = 0$; (b) $\delta_3 = 10\,\mu$eV. Inset: Polarization of the probe and control fields.

spectrum. In other words, a single exciton splits into two dressed excitons, and their energy difference is found to be proportional to the DDI. As the distance between the QD and graphene increases, the splitting decreases since the direct DDI term Π_i is inversely proportional to R^3. In Fig. 2(b), we have plotted the energy absorption rate when the control field is detuned such that $\delta_3 = 10\,\mu$eV. In this case, we find one peak and negligible electromagnetically induced transparency when R is large. When R decreases, the single peak splits into two peaks due to the DDI. These results show that the DDI can be used to split one exciton into two excitons, and also to control the electromagnetically induced transparency phenomenon.

In Fig. 3, we have investigated the effect of the photonic crystal on the energy absorption rate in the lambda-type QD. Initially, the lower band edge of the photonic crystal lies far away from the resonance energies of the QD (see solid curve), and there is weak coupling between the QD and photonic crystal. When we move the lower band edge closer to the resonance frequency ω_{13} of the QD, the two peaks in the power absorption spectrum merge into a broad peak with a narrow electromagnetically induced transparency window at $\delta_2 = 0$ (see dashed curve). Note also that the height of the peaks decreases. The merging of the split peaks in the QD power absorption spectrum occurs because the spontaneous decay rates become larger than the DDI splitting for the two peaks. The value of the decay rate is large because the photonic density of states is large when the resonance energy of the QD lies near the band edges. For example, we found $\Gamma_{21} = 6.40\,\mu$eV and $\Gamma_{31} = 3.81\,\mu$eV, whereas the energy splitting is about 2.80 μeV. Here, the location of the photonic crystal band edges can be changed by applying an intense pulsed laser field. The intense laser field causes the refractive index of polystyrene, an optical nonlinear material, to change due to the Kerr effect.

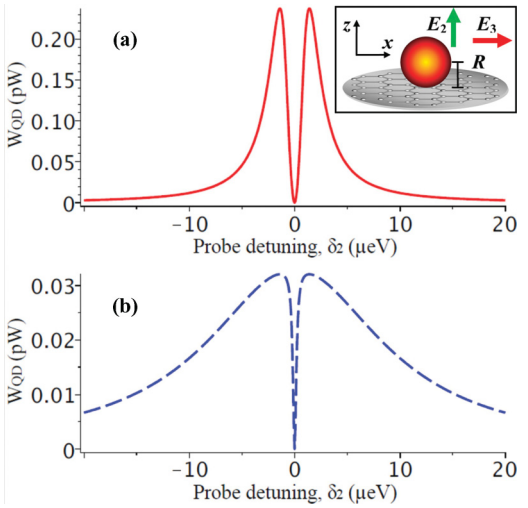

FIG. 3. (Color online) Energy absorption rate in the QD as a function of probe field detuning δ_2 when the lower band edge of the photonic crystal is taken as $\varepsilon_v = \hbar\omega_{12} + 17.88$ meV (a) and $\varepsilon_v = \hbar\omega_{12} + 0.56$ meV (b). Here, $R = 13$ nm and $\delta_3 = 0$. Inset: Polarization of the probe and control fields.

This change is quantified by the expression $n_a' = n_a + n_3 I_{\text{pump}}$ where n_3 is the Kerr nonlinearity constant and has the value $n_3 = 1.15 \times 10^{-12}$ cm^2/W for polystyrene.[10] For the pump field intensity $I_{\text{pump}} = 31.0$ GW/cm^2, we found that the photonic crystal band edge shifts such that $\Delta\varepsilon_v = -17.32$ meV. This means that the hybrid system can be used to study the nonlinear properties of photonic crystals. Using an external pump field to induce a large Kerr nonlinearity in the polystyrene photonic crystal is also an effective way to switch the energy transfer between two states, from high- to low-energy transfer peaks. Alternatively, the refractive index of the background material in the photonic crystal can also be modified by immersing the photonic crystal in another material. Therefore, the present QD-graphene system can also be used as a nanosensor.

We now investigate the energy transfer rate from the QD to graphene, and the results are plotted in Fig. 4 as a function of probe detuning when the QD-graphene separation R is varied. We find that the power transfer spectrum has a single peak with a narrow electromagnetically induced transparency

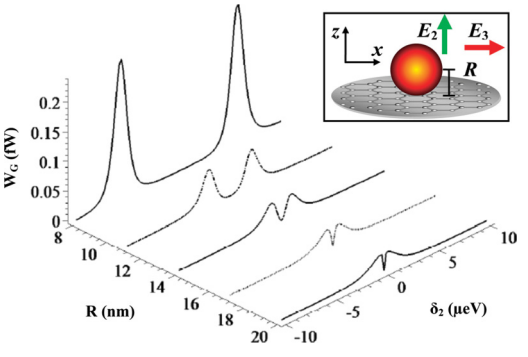

FIG. 4. (Color online) Energy transfer rate from the QD to graphene as a function of probe field detuning δ_2 when the QD-graphene nanodisk separation R is varied and $\delta_3 = 0$. Inset: Polarization of the probe and control fields.

window when R is large (i.e., $R = 20$ nm). When the QD is brought closer to graphene (i.e., $R = 8$ nm), the power transfer spectrum has one large minimum and two peaks with separation proportional to the DDI. This indicates that energy is transferred from the QD to the graphene when the two dressed excitons created in the QD are absorbed by graphene. This is an interesting finding, and can be used to transfer energy absorbed by the QD from a light source (i.e., the sun) to graphene where it can be stored. Therefore, one can fabricate energy transfer and storage devices (i.e., solar cells) from the present hybrid system.

It is also found that the height of the energy transfer peaks increases as the QD-graphene separation decreases (see Fig. 4). This effect has been observed experimentally by Chen *et al.*[31] and Dong *et al.*[32] They found that as the distance between CdTe QDs and a graphene oxide sheet decreases, there is a strong quenching of the QD fluorescence. They concluded that the fluorescence quenching could be due the energy transfer from the QD to the graphene sheet. For example, Chen *et al.*[31] deposited graphene on quartz substrates and then CdSe/ZnS QDs were deposited on graphene. The fluorescence measurements were performed on the individual QDs located both on the bare quartz substrate and on a graphene layer. They observed strong fluorescence quenching for QDs deposited on the graphene sheet, which was attributed to the energy transfer between QD and graphene and not due to photoinduced electron transfer from the QD to graphene. Similarly, Wang *et al.*[33] performed photoluminescence measurements on CdS QDs and ZnS QDs on graphene and observed a strong quenching of photoluminescence for these QDs due to the presence of the graphene sheet. They also performed transient photovoltaic experiments on their hybrid systems and found a very unexpected strong positive photovoltaic response due to the DDI. Conversely, it was found that separate samples of graphene and CdS QDs of a similar size do not show any photovoltaic response. They concluded that their experimental findings can be explained due to the energy transfer between the QD and the graphene sheet. Similar energy transfer between a QD and carbon nanotube has also been found experimentally by Shafran *et al.*[34]

When a QD is in contact with biomolecules, molecular beacons, DNA, or aptamers, its dielectric constant can be modified. Therefore, we have investigated the role of the dielectric constant of the QD on the energy transfer to graphene. The results are plotted in Fig. 5(a) for three values of ϵ_d. It is found that by changing the dielectric constant of the QD, the height of the energy transfer peaks can be modified. For example, by increasing or decreasing the dielectric constant, the height of the energy transfer spectra decreases or increases, respectively. This is because the energy transfer is inversely proportional to the square of the dielectric constant, as shown in Eq. (24). This effect has also been verified experimentally by Dong *et al.*,[32] where upon integrating a molecular beacon to a CdTe QD, it was found that the fluorescence quenching due to graphene is modified. We also note that at certain values of probe detuning, say for example, $\delta_2 \approx \pm 1.5$ μeV, the sensitivity of the energy transfer rate to the change in dielectric constant is quite high. This is an interesting finding, particularly if one considers that the present hybrid system can be used to fabricate nanobiosensors.

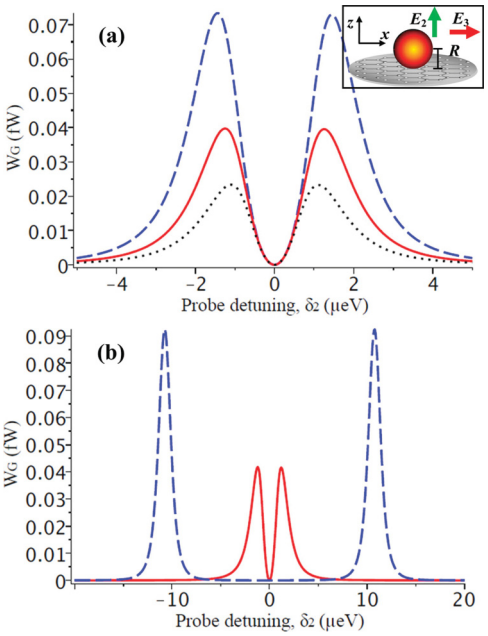

FIG. 5. (Color online) (a) Energy transfer rate from the QD to graphene when the dielectric function of the QD is taken as $\epsilon_d = 10$ (dotted curve), 12 (solid curve), and 14 (dashed curve). Here, $R = 13$ nm and $\delta_3 = 0$. (b) Energy transfer rate from the QD to graphene when the thickness of graphene is varied between one layer (solid curve) or two (dashed curve). Here, $R = 13$ nm and $\delta_3 = 0$. Inset: Polarization of the probe and control fields.

We have also studied the effect of the number of graphene layers on the energy transfer spectrum. In Fig. 5(b), we have plotted the energy transfer rate to graphene when a single graphene layer or two layers are considered. Here, the ratio $L_x/L_z = 20$ is preserved in order to keep the surface plasmon polariton resonance frequency constant. Note that for two layers of graphene, the height of the energy transfer peak increases. As we add additional layers of graphene, we increase its volume. In turn, the DDI between the QD and graphene is enhanced. Therefore, both the height of the peaks in the energy transfer spectrum and their splitting are increased. This effect has also been verified experimentally by Chen *et al.*,[31] where it was found that increasing the number of graphene layers in a CdSe/ZnS nanocrystal-graphene composite system enhanced the QD fluorescence quenching effect.

We now consider an alternative configuration for the QD-graphene nanocomposite system where both transitions $|2\rangle \leftrightarrow |1\rangle$ and $|3\rangle \leftrightarrow |1\rangle$ couple with the surface plasmons in the graphene nanodisk. In this configuration, we consider that both ω_{12} and ω_{13} are close to ω_{sp}^{x} and the transition dipole moments (fields) μ_{12} (probe field) and μ_{13} (control field) are aligned along the x and y directions, respectively. In Fig. 6(a), we have plotted the energy transfer rate from the QD to graphene as a function of the probe field detuning while varying R. Here, the physical parameters are the same as considered in our previous calculations. Note that we see two peaks due to the DDI effect as in the first configuration. Previously, the two peaks were symmetric, but in this case they are asymmetric. This is due to the self-induced DDI parameter Λ_2, which causes both peaks to shift towards positive detuning due to the change in the

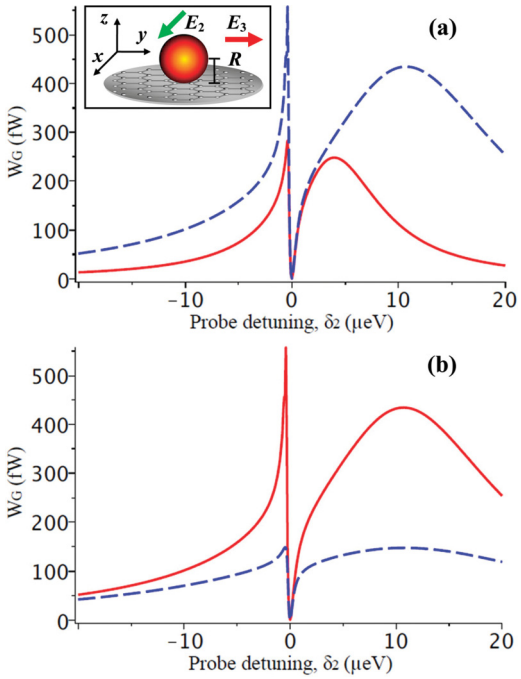

FIG. 6. (Color online) Energy transfer rate from the QD to graphene as a function of probe detuning δ_2 for the second configuration of dipole moments and fields (see inset). (a) The QD-graphene separation is varied from $R = 13$ nm (solid curve) to $R = 11$ nm (dashed curve). (b) $R = 11$ nm and the lower band edge of the photonic crystal is taken as $\varepsilon_v = \hbar\omega_{12} + 17.88$ meV (solid curve) and $\varepsilon_v = \hbar\omega_{12} + 0.56$ meV (dashed curve). Here, $\delta_3 = 0$. Inset: Polarization of the probe and control fields.

effective probe detuning from δ_2 to $\delta_2 + \Delta_{2d}$, as shown in Eq. (19). Here, also the width of both peaks increases due to the nonradiative decay Γ_{2d}. In the previous configuration, the self-induced DDI parameter Λ_2 was zero because there was no coupling between the QD transition $|2\rangle \leftrightarrow |1\rangle$ and graphene. These effects are enhanced by decreasing R.

In Fig. 6(b), the effect of the photonic crystal is investigated in the same way as in Fig. 3, and similar results are found as for the previous configuration. By applying an external pump laser field to the polystyrene photonic crystal, the power transfer to graphene can be switched from high to low values. We note that due to the asymmetry of the power transfer spectrum in this configuration, the sensitivity of this switching effect can change drastically depending on the value of probe field detuning. For example, negative detunings close to $\delta_2 = 0$ show a sharp peak in the energy transfer spectrum when the pump field is absent, and this peak is suppressed when the pump field is applied.

Finally, we investigate the energy absorption rate in a ladder-type QD coupled with the graphene nanodisk. The formulation for this system is given in the Appendix. We consider the case where the control field is coupled with the QD transition $|2\rangle \leftrightarrow |3\rangle$ and the graphene nanodisk, while the probe field is only coupled to the QD transition $|1\rangle \leftrightarrow |2\rangle$. Here, the resonance frequency ω_{23} lies near ω_{sp}^x, while ω_{12} is uncoupled from both ω_{sp}^x and ω_{sp}^z. This situation is analogous to that explored in Fig. 2 for the lambda-type QD. In Fig. 7, the

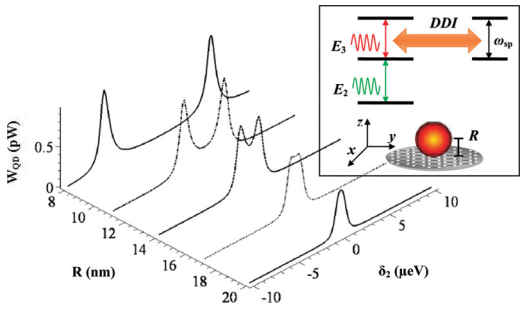

FIG. 7. (Color online) Energy absorption rate of to the ladder-type QD as a function of probe field detuning δ_2 when the QD-graphene nanodisk separation R is varied. Here, $\hbar\omega_{23} = 0.8036$ eV and the intensities of the probe and control fields are 1.0 and 3.0 W/cm^2, respectively. Other parameters are the same as considered previously. Inset: Schematic of the QD-graphene hybrid system with ladder-type energy level structure. Here, DDI coupling occurs only for the $|2\rangle \leftrightarrow |3\rangle$ transition.

energy absorption rate in the ladder-type QD is plotted when the QD-graphene nanodisk separation R is varied. We find that the power absorption spectrum gives two peaks and a minimum when R is small (i.e., $R = 8$ nm), as was found in Fig. 2. Note that for the ladder-type QD, the narrow minima due to electromagnetically induced transparency do not appear. This is because the same electromagnetically induced transparency effect does not appear in ladder-type systems.[39] We have also investigated the effect of the photonic crystal on the energy absorption rate in the ladder-type QD, and the results are shown in Fig. 8. Again, we consider that a pump field of intensity 31.0 GW/cm^2 is applied, which causes the photonic crystal band edge to shift and increases the decay rate of the QD. Note that the power absorption spectrum merges into a broad peak in the same way as it did for the lambda-type QD

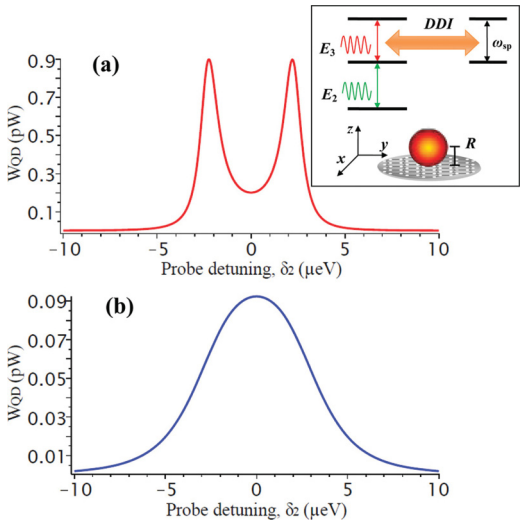

FIG. 8. (Color online) Energy absorption rate of the ladder-type QD as a function of probe field detuning δ_2 when the lower band edge of the photonic crystal is taken as $\varepsilon_v = \hbar\omega_{23} + 17.88$ meV (a) and $\varepsilon_v = \hbar\omega_{23} + 0.10$ meV (b). Here, $R = 10$ nm, $\delta_3 = 0$, and other parameters are the same as in Fig. 7. Inset: Schematic of the QD-graphene hybrid system with ladder-type energy level structure. Here, DDI coupling occurs only for the $|2\rangle \leftrightarrow |3\rangle$ transition.

[see Fig. 3(b)]. Here, however, the narrow minima present in the lambda-type QD are absent and we clearly see two peaks merging into one.

IV. CONCLUSIONS

We have investigated the dipole-dipole interaction (DDI) and energy transfer in a QD-graphene nanodisk system embedded within a photonic crystal. Our simulations predict that in this system, multiple excitonic states (dressed states) can be created in the quantum dot and then transferred to graphene with different frequencies. This phenomenon occurs purely due to the DDI between the QD and graphene, and results in energy transfer. We have demonstrated that the energy absorption of the QD and/or the energy transfer from the QD to graphene can be switched on and off by changing the strength of the DDI or by applying an intense external field to the photonic crystal. We have also verified our findings qualitatively with recent experimental data on energy transfer in QD-graphene nanocomposite systems. Our numerical results provide motivation for future experimental and theoretical investigations on nanocomposites made from graphene, carbon nanotubes, quantum dots, and photonic crystals. The present theory can be applied to hybrid systems consisting of graphene with quantum emitters such as quantum dots, nanocrystals, atoms, and chemical or biological molecules; the only requirement is that the quantum emitter should have at least three states. The proposed nanocomposite system can be used to fabricate nanosensors, all-optical nanoswitches, energy transfer devices, and energy storage devices.

ACKNOWLEDGMENTS

F.C. and M.A.A. acknowledge financial support from Project No. FIS2010-22082 from the Ministry of Science and Education of Spain.

APPENDIX

We consider a three-level quantum dot in the ladder configuration, where $|1\rangle$, $|2\rangle$, and $|3\rangle$ denote the ground, first excited, and second excited states, respectively. The probe field with amplitude E_2 and frequency ω_2 is coupled between states $|1\rangle$ and $|2\rangle$, while the control field with amplitude E_3 and frequency ω_3 is coupled between states $|2\rangle$ and $|3\rangle$. The decay of level $|2\rangle$ to level $|1\rangle$ (level $|3\rangle$ to level $|2\rangle$) is given as Γ_{21} (Γ_{32}). Using the same methods as for the lambda-type system, the density matrix equations of motion for the ladder-type energy level configuration are then obtained as

$$\frac{d\rho_{22}}{dt} = -\Gamma_{21}\rho_{22} + \Gamma_{32}\rho_{33} + iR_2e^{-i\theta_2}\rho_{21} + i\Lambda_2^*\rho_{12}\rho_{21} - iR_2e^{i\theta_2}\rho_{12} - i\Lambda_2\rho_{21}\rho_{12} - iR_3e^{-i\theta_3}\rho_{32} - i\Lambda_3^*\rho_{23}\widetilde{\rho}_{32} + iR_3e^{i\theta_3}\rho_{23} + i\Lambda_3\rho_{32}\rho_{23}, \quad \text{(A1)}$$

$$\frac{d\rho_{33}}{dt} = -\Gamma_{32}\rho_{33} + iR_3e^{-i\theta_3}\rho_{32} + i\Lambda_3^*\rho_{23}\rho_{32} - iR_3e^{i\theta_3}\rho_{23} - i\Lambda_3\rho_{32}\rho_{23}, \quad \text{(A2)}$$

$$\frac{d\rho_{21}}{dt} = d_{21}\rho_{21} + iR_2e^{i\theta_2}(\rho_{22} - \rho_{11}) - iR_3e^{-i\theta_3}\rho_{31} - i\Lambda_3^*\rho_{23}\rho_{31}, \quad \text{(A3)}$$

$$\frac{d\rho_{32}}{dt} = d_{32}\rho_{32} + iR_3e^{i\theta_3}(\rho_{33} - \rho_{22}) + iR_2e^{-i\theta_2}\rho_{31} + i\Lambda_2^*\rho_{12}\rho_{31}, \quad \text{(A4)}$$

$$\frac{d\rho_{31}}{dt} = (i\delta_2 + i\delta_3 - \Gamma_{32})\rho_{31} - iR_3e^{i\theta_3}\rho_{21} - i\Lambda_3\rho_{32}\rho_{21} + iR_2e^{i\theta_2}\rho_{32} + i\Lambda_2\rho_{21}\rho_{32}, \quad \text{(A5)}$$

where

$$d_{21} = i\delta_2 + i\Delta_{2d} - \Gamma_{21} - \Gamma_{2d},$$
$$d_{32} = i\delta_3 + i\Delta_{3d} - \Gamma_{32} - \Gamma_{3d},$$

and

$$\Delta_{2d} = \mathrm{Re}(\Lambda_2)(\rho_{22} - \rho_{11}),$$
$$\Gamma_{2d} = \mathrm{Im}(\Lambda_2)(\rho_{22} - \rho_{11}),$$
$$\Delta_{3d} = \mathrm{Re}(\Lambda_3)(\rho_{33} - \rho_{22}),$$
$$\Gamma_{3d} = \mathrm{Im}(\Lambda_3)(\rho_{33} - \rho_{22}).$$

In the above expressions, all quantities are the same as given previously for the lambda-type system but with the substitutions $\omega_{13} \to \omega_{23}, \mu_{13} \to \mu_{23}$, and $\Gamma_{31} \to \Gamma_{32}$. The QD energy absorption rate and the power transfer in this system are calculated using Eqs. (23) and (24) with the subsitutions $\rho_{11} \to \rho_{ii}, \rho_{13} \to \rho_{23}$.

[1] M. Achermann, J. Phys. Chem. Lett. **1**, 2837 (2010).
[2] R. D. Artuso and G. W. Bryant, Phys. Rev. B **82**, 195419 (2010).
[3] S. M. Sadeghi, L. Deng, X. Li, and W.-P. Huang, Nanotechnology **20**, 365401 (2009).
[4] M.-T. Cheng, S.-D. Liu, H.-J. Zhou, Z.-H. Hao, and Q.-Q. Wang, Opt. Lett. **32**, 2125 (2007).
[5] M. Durach, A. Rusina, V. I. Klimov, and M. I. Stockman, New J. Phys. **10**, 105011 (2008).
[6] J. M. Luther, P. K. Jain, T. Ewers, and A. P. Alivisatos, Nat. Mater. **10**, 361 (2011).
[7] J. D. Joannopoulos, S. G. Johnson, J. N. Winn, and R. D. Meade, *Photonic Crystals: Molding the Flow of Light*, 2nd ed. (Princeton University Press, Princeton, New Jersey, 2008).
[8] A. Chutinan, S. John, and O. Toader, Phys. Rev. Lett. **90**, 123901 (2003).
[9] Y. Liu, F. Qin, Z.-Y. Wei, Q.-B. Meng, D.-Z. Zhang, and Z.-Y. Li, Appl. Phys. Lett. **95**, 131116 (2009).
[10] F. Qin, Y. Liu, and Z.-Y. Li, J. Opt. **12**, 035209 (2010).
[11] J. D. Cox and M. R. Singh, J. Appl. Phys. **108**, 083102 (2010).
[12] N. Tétreault, E. Arsenault, L.-P. Heiniger, N. Soheilnia, J. Brillet, T. Moehl, S. Zakeeruddin, G. A. Ozin, and M. Gratzel, Nano Lett. **11**, 4579 (2011).
[13] C. E. Talley, J. B. Jackson, C. Oubre, N. K. Grady, C. W. Hollars, S. M. Lane, T. R. Huser, P. Nordlander, and N. J. Halas, Nano Lett. **5**, 1569 (2005).

[14]N. I. Zheludev, Opt. Photon. News **22**, 30 (2011).
[15]H. A. Atwater and A. Polman, Nat. Mater. **9**, 205 (2010).
[16]L. Novotny and N. Van Hulst, Nat. Photonics **5**, 83 (2011).
[17]A. Gonzalez-Tudela, D. Martin-Cano, E. Moreno, L. Martin-Moreno, C. Tejedor, and F. J. Garcia-Vidal, Phys. Rev. Lett. **106**, 020501 (2011).
[18]P. R. West, S. Ishii, G. V. Naik, N. K. Emani, V. M. Shalaev, and A. Boltasseva, Laser Photonics Rev. **4**, 795 (2010).
[19]A. H. Castro Neto, F. Guinea, N. M. R. Peres, K. S. Novoselov, and A. K. Geim, Rev. Mod. Phys. **81**, 109 (2009).
[20]F. Bonaccorso, Z. Sun, T. Hasan, and A. C. Ferrari, Nat. Photonics **4**, 611 (2010).
[21]F. Schedin, E. Lidorikis, A. Lombardo, V. G. Kravets, A. K. Geim, A. N. Grigorenko, K. S. Novoselov, and A. C. Ferrari, ACS Nano **4**, 5617 (2010).
[22]F. H. L. Koppens, D. E. Chang, and F. J. G. Abajo, Nano Lett. **11**, 3370 (2011).
[23]K. P. Loh, Q. Bao, G. Eda, and M. Chhowalla, Nat. Chem. **2**, 1015 (2010).
[24]R. R. Nair, P. Blake, A. N. Grigorenko, K. S. Novoselov, T. J. Booth, T. Stauber, N. M. R. Peres, and A. K. Geim, Science **320**, 1308 (2008).
[25]T. Mueller, F. Xia, and P. Avouris, Nat. Photonics **4**, 297 (2010).
[26]M. Jablan, H. Buljan, and M. Soljacic, Phys. Rev. B **80**, 245435 (2009).
[27]Q. Bao, H. Zhang, B. Wang, Z. Ni, C. H. Y. X. Lim, Y. Wang, D. Y. Tang, and K. P. Loh, Nat. Photonics **5**, 411 (2011).
[28]C. Tegenkamp, H. Pfnur, T. Langer, J. Baringhaus, and H. W. Schumacher, J. Phys.: Condens. Matter **23**, 012001 (2011).
[29]A. Manjavacas, P. Norlander, and F. J. G. Abajo, ACS Nano **6**, 1724 (2012).
[30]A. Cao, Z. Liu, S. Chu, M. Wu, Z. Ye, Z. Cai, Y. Chang, S. Wang, Q. Gong, and Y. Liu, Adv. Mater. **22**, 103 (2010).
[31]Z. Chen, S. Berciaud, C. Nuckolls, T. F. Heinz, and L. E. Brus, ACS Nano **4**, 2964 (2010).
[32]H. Dong, W. Gao, F. Yan, H. Ji, and H. Ju, Anal. Chem. (Washington, DC) **82**, 5511 (2010).
[33]P. Wang, T. Jiang, C. Zhu, Y. Zhai, D. Wang, and S. Dong, Nano Res. **3**, 794 (2010).
[34]E. Shafran, B. D. Mangum, and J. M. Gerton, Nano Lett. **10**, 4049 (2010).
[35]G. Goncalves, P. A. A. P. Marques, C. M. Granadeiro, H. I. S. Nogueira, M. K. Singh, and J. Gracio, Chem. Mater. **21**, 4796 (2009).
[36]C. Xu, X. Wang, and J. Zhu, J. Phys. Chem. C **112**, 19841 (2008).
[37]R. Patakfalvi, D. Diaz, P. Santiago-Jacinto, G. Rodriguez-Gattorno, and R. Sato-Berru, J. Phys. Chem. C **111**, 5331 (2007).
[38]S. Evangelou, V. Yannopapas, and E. Paspalakis, Phys. Rev. A **83**, 023819 (2011); **83**, 055805 (2011); V. Yannopapas, E. Paspalakis, and N. V. Vitanov, Phys. Rev. Lett. **103**, 063602 (2009).
[39]M. O. Scully and M. S. Zubairy, *Quantum Optics* (Cambridge University Press, Cambridge, UK, 1997).
[40]M. Fleischhauer, A. Imamoglu, and J. P. Marangos, Rev. Mod. Phys. **77**, 633 (2005).
[41]M. V. Gurudev Dutt, J. Cheng, B. Li, X. Xu, X. Li, P. R. Berman, D. G. Steel, A. S. Bracker, D. Gammon, S. E. Economou, R.-B. Liu, and L. J. Sham, Phys. Rev. Lett. **94**, 227403 (2005).
[42]X. Xu, B. Sun, P. R. Berman, D. G. Steel, A. S. Bracker, D. Gammon, and L. J. Sham, Nat. Phys. **4**, 692 (2008).
[43]J. M. Elzerman, K. M. Weiss, J. Miguel-Sanchez, and A. Imamoglu, Phys. Rev. Lett. **107**, 017401 (2011).
[44]D. Sarid and W. A. Challener, *Modern Introduction to Surface Plasmons: Theory, Mathematica Modeling, and Applications* (Cambridge University Press, New York, 2010).
[45]P. Hanarp, M. Käll, and D. S. Sutherland, J. Phys. Chem. B **107**, 5768 (2003).
[46]C. Langhammer, M. Schwind, B. Kasemo, and I. Zorić, Nano Lett. **8**, 1461 (2008).
[47]C. F. Bohren and D. R. Huffman, *Absorption and Scattering of Light by Small Particles* (Wiley, New York, 1983), Chap. 5.
[48]E. C. Le Ru, *Principles of Surface-Enhanced Raman Spectroscopy and Related Plasmonic Effects* (Elsevier, Amsterdam, 2009), Appendix G.
[49]B. E. Kane, Phys. Rev. B **82**, 115441 (2010).
[50]S. John and J. Wang, Phys. Rev. B **43**, 12772 (1991).
[51]I. Haque and M. R. Singh, J. Phys.: Condens. Matter **19**, 156229 (2007).
[52]S. Thongrattanasiri, A. Manjavacas, and F. J. G. de Abajo, ACS Nano **6**, 1766 (2012).